



ORIGINAL ARTICLE

Emilio Barchiesi · Stefanos Mavrikos · Ivan Giorgio ·  
Costas Grigoropoulos · Maria Farsari · Francesco dell'Isola ·  
Gordon Zyla

# Complex mechanical properties of 3D micro-metric pantographic metamaterials fabricated by two-photon polymerization

Received: 21 July 2024 / Accepted: 28 August 2024

© The Author(s), under exclusive licence to Springer-Verlag GmbH Germany, part of Springer Nature 2024

**Abstract** Mechanical metamaterials consist of specially engineered features designed to tailor and enhance the mechanical properties of their constituent materials. In this context, 2D pantographic fabrics have gained attention for their unique deformation behavior, providing remarkable resilience and damage tolerance. This study explores micro-metric metamaterials with 3D pantographic motifs, aiming to transfer these properties to small scales. 3D micro-metric structures were designed using 2D pantographic fabrics arranged in multiple layers, each featuring unit cells with quasi-perfect pivots. Relatively large specimens of 3D micro-metric pantographs, measuring  $158\ \mu\text{m} \times 250\ \mu\text{m} \times 450\ \mu\text{m}$ , were fabricated in various configurations using two-photon polymerization. These specimens were mechanically characterized through in-situ scanning electron microscopy microindentation under conditions of cyclic deformation. Structural failures were subsequently assessed via helium-ion microscopy. The 3D micro-metric pantographs exhibited complex mechanical properties, some aligning with those of 2D pantographic fabrics, while new properties, such as a dissipative response and softening, were identified. Nonetheless, the 3D micro-metric pantographs demonstrated great resilience against deformation and enhanced resistance to undesired out-of-plane motions, indicating their potential for novel applications in advanced engineering fields. Additionally, the findings can potentially lead to optimizing and enriching theoretical models describing the mechanical behavior of pantographic metamaterials.

**Supplementary Information** The online version contains supplementary material available at <https://doi.org/10.1007/s00161-024-01327-y>.

E. Barchiesi  
Department of Architecture, Design and Urban Planning, University of Sassari, Alghero, Italy

S. Mavrikos · C. Grigoropoulos  
Department of Mechanical Engineering, University of California, Berkeley, USA

I. Giorgio · F. dell'Isola  
Department of Civil, Construction-Architectural and Environmental Engineering, University of L'Aquila, L'Aquila, Italy

M. Farsari · G. Zyla (✉)  
Institute of Electronic Structure and Laser, Foundation for Research and Technology-Hellas, Heraklion, Greece  
e-mail: [zyla@iesl.forth.gr](mailto:zyla@iesl.forth.gr)

F. dell'Isola  
Faculty of Mechanical and Industrial Engineering, Warsaw University of Technology, Warsaw, Poland

F. dell'Isola  
Ecole Normale Supérieure Paris Saclay, Paris, France

F. dell'Isola  
International Research Center for the Mathematics and Mechanics of Complex Systems, University of L'Aquila, L'Aquila, Italy

**Keywords** Mechanical metamaterials · Two-photon polymerization · Pantographic structures · In-situ SEM microindentation

## 1 Introduction

Traditional materials employed in engineering are struggling to meet the increasing demands of advanced applications. As a result, there is a growing need for innovative materials with enhanced properties. Recent advances in manufacturing techniques now enable intricate manipulation of materials at various scales [1,2]. These advancements have facilitated precise control over engineered microstructures, involving the arrangement of matter through architected unit cells. Such intentionally designed materials, commonly referred to as metamaterials [3], display exceptional acoustic and mechanical behaviors, surpassing the inherent properties of their constituent materials, thereby positioning metamaterials at the forefront of modern engineering.

Among the most highly regarded unit cell architectures in mechanical metamaterials are auxetics and pentamodes. Both theoretically and experimentally, these architectures have demonstrated extraordinary structural behaviors, such as a negative Poisson's ratio [4] and a low shear modulus [5]. Additionally, various truss lattices have also displayed exceptional structural behaviors, particularly robust ultralight properties [6].

The term 'auxetic,' introduced by Evans et al. in 1991 [7], describes materials that expand in the direction perpendicular to the applied load when subjected to uniaxial tensile stress.

Pentamodes-materials that maintain their volume under minor deformations-presented a novel approach for creating metamaterials with elastic properties determined by a desired elasticity tensor, within the framework of Cauchy mechanics [8]. In this context, they introduced the concept of "extremal metamaterials," which exhibit remarkable stiffness under specific deformation modes while being highly compliant under others. Given that the strain tensor has six independent components in three-dimensional space, 3D extremal metamaterials can be categorized into seven groups based on their compliance with deformation modes: null-mode, uni-mode, bi-mode, tri-mode, quadra-mode, penta-mode, and hexa-mode.

Recently, a new class of 2D fabric architectures known as pantographs has garnered attention in the field of mechanical metamaterials. This interest is particularly driven by their unique deformation energy, which originates from their structural composition that comprises two families of mutually orthogonal beams connected by (quasi-)perfect pivots [9]. The deformation behavior of these networks predominantly follows a second-gradient energy pattern [10,11]. This suggests that pantographic fabrics can be theoretically modeled using generalized continua, particularly those of the second-gradient type<sup>1</sup> [12–14]. As a result, pantographic fabrics have rekindled research interest in generalized continua within the field of metamaterials. This resurgence is due to their ability to explain phenomena such as size effects, the existence of zero-energy modes, and the impact of non-local interactions-issues often overlooked in classical first-gradient theories, or more precisely, in Cauchy mechanics [9].

The mathematical models based on generalized continua have effectively captured the unique properties of 2D pantographic metamaterials. These properties have been experimentally validated through various additive manufacturing techniques, using diverse materials, such as metals and polymers [15]. A comprehensive overview of scientific and technological advancements related to fabrics with pantographic motifs is available in Ref. [15,16]. Initial studies employed additive manufacturing to create specimens at centimeter and millimeter scales [17–20]. Subsequent research successfully fabricated even smaller specimens, comprising just a few pantographic unit cells, at the micrometer scale [21,22].

Key findings from these studies suggest that well-designed pantographic fabrics display exceptional elastic behavior. This property is attributed to the quasi-zero-energy modes inherent in the pantographic design. This unique characteristic causes the fabrics to primarily bend rather than extend until the onset of the first rupture under applied deformation.

Interestingly, when initial defects are absent and quasi-perfect pivots are employed, the first rupture may not necessarily occur at the points of maximum elongation. Instead, it could take place at the pivots connecting features from different families; the most sheared regions of the specimens often correspond to areas where pivot torsion is at its peak. However, in pantographic fabrics with quasi-perfect pivots, damage mechanisms are significantly influenced by geometric dimensions and the properties of the raw material as described in Ref. [17].

In general terms, pantographic fabrics, whether equipped with perfect or quasi-perfect pivots, exhibit highly damage-tolerant behavior. This resilience can be attributed to their reticulated structure, enabling effective load

<sup>1</sup> In the sense that the weight of the second-gradient terms in the strain energy exceeds that of the first-gradient terms.

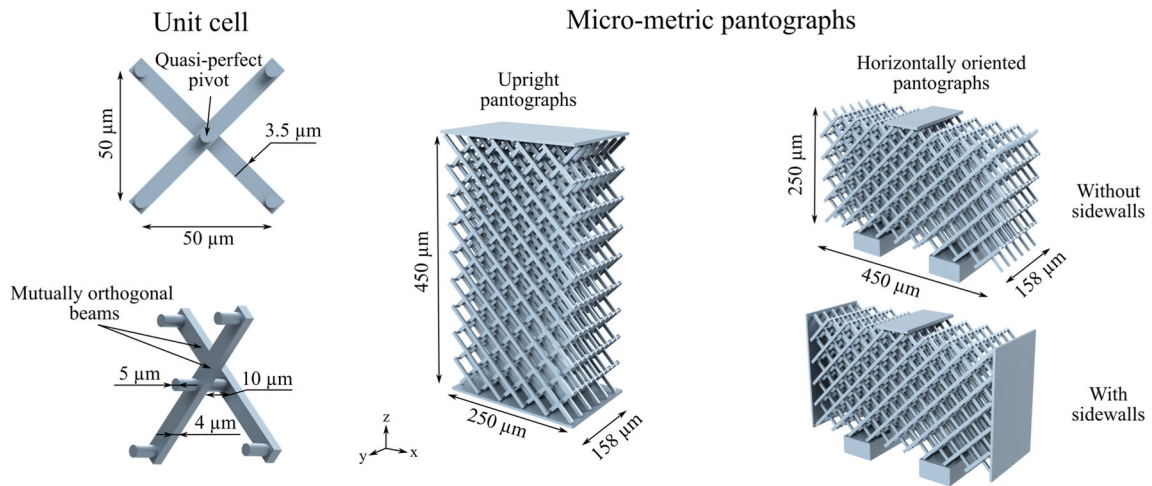


**Fig. 1** Design of 3D micro-metric pantographs. A pantographic unit cell, along with its significant geometrical parameters, is illustrated on the left. It consists of two families of mutually orthogonal beams interconnected by quasi-perfect pivots. Additional pivots are insert to provide a better understanding of the interconnection of pantographic unit cells in a 3D environment. The unit cells were utilized to create 3D specimens in both upright and horizontal orientations, all having the same dimensions

redistribution among intact features [23]. Remarkably, pantographic fabric metamaterials at centimeter, millimeter, and micrometer scales show nearly identical mechanical behavior. This observation strongly supports the notion that 2D pantographs are indeed metamaterials. Moreover, their elastic and post-elastic properties seem to be minimally influenced by the raw material and length scale, introducing exciting possibilities for their use at extremely fine scales [15].

Motivated by the aim of advancing the field of pantographic metamaterials, this paper explores the mechanical characteristics of assembling multiple layers of 2D pantographic fabrics with quasi-perfect pivots into 3D micro-metric pantographs. This research aims to foster the utilization of these structures in potential applications, specifically at extremely small length scales, such as micro-electromechanical systems (MEMS). Therefore, the present research examines whether the scale-invariant mechanical behavior typically observed in 2D pantographic fabrics also persists in the proposed 3D specimens. Different deformation patterns are investigated through various configurations of 3D micro-metric structures, considering the presence and absence of lateral reinforcements. This investigation is crucial because external forces, structural features and material properties may become increasingly significant at the micro-/nanoscale due to intermolecular interactions, potentially altering the anticipated mechanisms of 3D micro-metric pantographs.

To address these objectives, 3D structures were fabricated using two-photon polymerization (2PP), an advanced laser-based 3D printing technique that offers sub-micron resolution [24–26]; 2PP has been widely recognized as a superior fabrication tool across various disciplines, including biophotonics [27,28], photonics [29,30], biomimetics [31,32], and optics [33,34].

To characterize the mechanical properties of the 3D micro-metric pantographs, loading-unloading tests were conducted using in-situ scanning electron microscope (SEM) microindentation. These tests focused on relatively large deformations and cyclic conditions. Structural failures were assessed through helium-ion microscopy (HIM).

## 2 Design of 3D micro-metric pantographic metamaterials

To examine the potential scale-invariant mechanical behavior of 3D micro-metric pantographs in relation to different deformation patterns and other influential factors on their mechanical properties, three different types of 3D micro-metric pantographs with quasi-perfect pivots were designed using the commercially available CAD software, Autodesk Fusion 360. These include an upright pantograph and two horizontally oriented pantographs, with their significant geometrical parameters illustrated in Fig. 1. Here, it is worth noting that the term “3D” is used solely to describe the arrangement of unit cells in all three dimensions. However, from a mechanical perspective, these pantographs could be more appropriately termed 2.5D materials, as they consist of multiple layers of 2D pantographic fabrics.

Specifically, the upright pantograph was placed between two plates to facilitate compression tests. Each plate had a thickness of  $5\ \mu\text{m}$  and covered an area of  $250\ \mu\text{m} \times 160\ \mu\text{m}$ . In contrast, the horizontally oriented pantographs were constructed on two blocks, each measuring  $75\ \mu\text{m} \times 160\ \mu\text{m} \times 40\ \mu\text{m}$ . A plate centrally located atop these structures and measuring  $80\ \mu\text{m} \times 165\ \mu\text{m} \times 5\ \mu\text{m}$  facilitated the three-point bending tests of the 3D pantographic structures. Furthermore, one of the horizontally oriented pantographs featured sidewalls with dimensions identical to the plates used in the upright configuration to evaluate the impact of lateral reinforcement on the effective stiffness of the specimens.

The relative dimensions for the unit cell were estimated to align with pantographic fabrics studied at different length scales [15], aiming to achieve sufficient bending properties for exploring mechanical behavior at extremely small scales. The overall dimensions of the pantographs were determined based on constraints related to the manufacturing process, such as fabrication time, resolution, and processable area.

### 3 Methods and materials for the fabrication and characterization of 3D micro-metric pantographic metamaterials

3D micro-metric pantographic metamaterials were fabricated using 2PP with an optical setup illustrated in Fig. 2A. A fiber laser system (FemtoFiber ultra 780, Toptica Photonics AG) emitted laser radiation with a central wavelength of 780 nm, pulse duration of 150 fs, and a repetition rate of 80 MHz. To focus the laser beam into the photosensitive material, a microscope objective (20x/NA 0.8, Plan-Apo, Zeiss, Germany) was used, as shown in Fig. 2B.

The photosensitive material selected for this work was SZ2080<sup>TM</sup>, a hybrid organic–inorganic photopolymer known for its high-resolution 3D printing capabilities and minimal shrinkage [35,36]. SZ2080<sup>TM</sup> comprises two organic photopolymerizable monomers: Methacryloxypropyl trimethoxysilane (MAPTMS, 99%, Sigma-Aldrich, Germany) and methacrylic acid (MAA, 98%, Sigma-Aldrich, Germany). An inorganic network is formed by Zirconium n-propoxide (ZPO, 70%, Sigma-Aldrich, Germany) and the alkoxy silane groups from MAPTMS. 4,4'-bis(diethylamino) benzophenone (Michler's ketone, Sigma-Aldrich, Germany) served as the photoinitiator.

After the synthesis of SZ2080<sup>TM</sup> via the sol–gel process [37], a vacuum atmosphere was applied to 2 ml of SZ2080<sup>TM</sup> for a duration of 12 h to increase the material's viscosity. This step facilitated precise drop-casting, thereby ensuring the desired droplet height for processing large pantographic metamaterial specimens. SZ2080<sup>TM</sup> was drop-casted onto silanized coverslips (Deltalab, Spain) measuring 22 mm x 22 mm in size and their thickness ranging between  $130\ \mu\text{m}$  and  $160\ \mu\text{m}$ . The process of silanization was employed to enhance the adhesion of 2PP-processed structures to the substrate [37]. Finally, the sample was placed in a vacuum atmosphere for an additional 72 h to enable the evaporation of any remaining solvents before 2PP processing.

The fabrication of pantographic metamaterials using 2PP was carried out layer-by-layer, using the commercially available software Arachne (Biomimetic, Greece). Prior to 2PP, the exposure paths were defined by slicing and hatching the 3D computer models of the specimens. This slicing and hatching process was performed using Istos (Biomimetic., Greece) at a resolution of 200 nm. A 2D galvo scanner (hurryscan II 10, Scanlab, Germany) and a shutter (MTS40-A3–750.850, AA Opto Electronics, France) were employed to produce each layer with its specific geometry. The galvo scanner was further augmented by a lens system to extend the processable field-of-view of the microscope objective, as described in Ref. [38]. All structures were processed using an average laser power of 120 mW, measured directly after the shutter. The galvo scanner speed was 150 mm/s.

Upon completing the processing of one layer, the sample was moved along the z-axis using a linear stage (M-605.1DD, Physik Instrumente, Germany) to prepare for the processing of the next layer. Two additional linear stages of the same model facilitated the horizontal shifting of the sample in the x and y directions, enabling the fabrication of multiple specimens within a single droplet of SZ2080<sup>TM</sup>.

To avoid focusing the laser beam through previously polymerized material, pantographic structures were processed in a top-down approach (see Fig. 2B), in which the “top” refers to the upper surface of the structures. After completing the 2PP process, the sample was immersed in 4-methyl-2-pentanone (Sigma-Aldrich, Germany) for 45 min to remove any material not exposed to the laser radiation. This step was followed by a 10-minute immersion in isopropanol (Sigma-Aldrich, Germany) to clean the glass substrate.

The mechanical properties of 3D micro-metric pantographs were assessed through loading-unloading tests, employing in-situ SEM (Scios 2 Dual Beam, Thermo Fisher Scientific, United States) microindentation (Hysitron PI 88, Bruker, United States). Beforehand, the structures were sputter-coated with a 10 nm thick



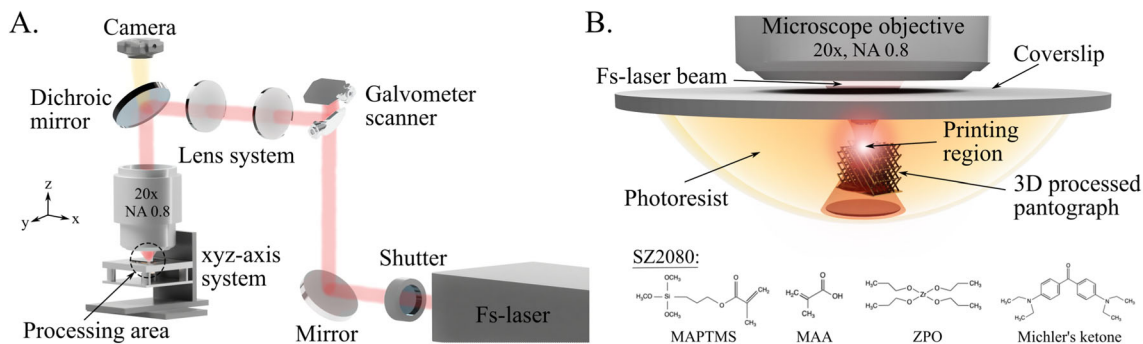


**Fig. 2** Fabrication of 3D micro-metric pantographic metamaterials using 2PP. **A** Schematic illustration of the 2PP setup. **B** A detailed view of the processing area in 2PP and illustration of the chemical composition of the hybrid photoresist SZ2080

Pd/Au-film. A laser-processed flat punch with a diameter of 200  $\mu\text{m}$  was employed for the microindentation. Such experiments were conducted under displacement control to mitigate creep effects, as described in Ref. [39].

The maximum displacement was set to 50  $\mu\text{m}$  for upright pantographic metastructures for compression test and 25  $\mu\text{m}$  for those oriented horizontally for three-point bending tests. The displacement velocity was consistently maintained at 5  $\mu\text{m/s}$ . The maximum applied displacement of the pantographic structures was held for 500 ms before unloading was initialized at the same speed. This cycle was repeated 20 times for each specimen. Although the structures were not preloaded, an initial loading-unloading test was carried out to ensure the proper alignment of the flat punch with the micro-metric pantographs. It should be noted that during this initial test, the structures were not compressed to the aforementioned maximum displacement values; instead, the applied deformation remained within the elastic region.

Subsequent to loading-unloading tests, the structures underwent examination for potential structural failures using HIM (ORION NanoFab, Zeiss, Germany), without a second sputter-coating of the samples.

#### 4 Mechanical properties of 3D micro-metric pantographic metamaterial

Unloaded 3D micro-metric pantographic metamaterials, processed by 2PP, are illustrated in the SEM images on the left, as depicted in Fig. 3. The structures showed high-quality and high resolution and the overall dimensions of the structures aligned well with those mentioned in the designed 3D models (see Fig. 1). The center SEM images in Fig. 3 demonstrate how the pantographs were deformed under loading using the flat punch. The videos of the cyclical microindentation tests can be accessed in the supplementary files.

The upright pantograph, as illustrated in Fig. 3A, undergoes a unique deformation pattern when subjected to a compression test. The areas of the specimen confined by the two red triangles exhibit nearly rigid behavior (see Fig. 3B). This rigidity arises because all the features within these regions intersect and attach to the plates used to sandwich the structure, which serves as a clamp. Due to the highly constrained kinematics of the pantographic unit cells, these red regions experience minimal deformation. In contrast, the area marked by the green rhombus, where the features are not directly attached to any constraints, undergoes the maximum shear deformation, i.e., the change in the relative angle between intersecting features is at its highest. As seen in Fig. 3B, feature bending is concentrated at the boundaries of both the red and green regions. The thickness of these boundaries is thus determined by the bending stiffness of the features, which can be described using a second-gradient type continuum model.

Horizontally-oriented pantographic metamaterials, as shown in Fig. 3D and G, were subjected to a three-point bending test and exhibited a deformation pattern distinct from that of upright pantographs. This difference is attributed to the varying constraints applied to the pantographic unit cells in a three-point bending test. As previously mentioned, this test aimed to assess the role of lateral reinforcement on the effective stiffness of the 3D micro-metric pantographs. However, under such load conditions, the mechanical properties of 3D micro-metric pantographs with sidewalls (see Fig. 3E and H) did not significantly differ from that observed for specimens without sidewalls. Although the sidewalls were not perfectly fabricated, displaying minor local detachment, the mechanical tests revealed that the presence or absence of sidewalls does not significantly

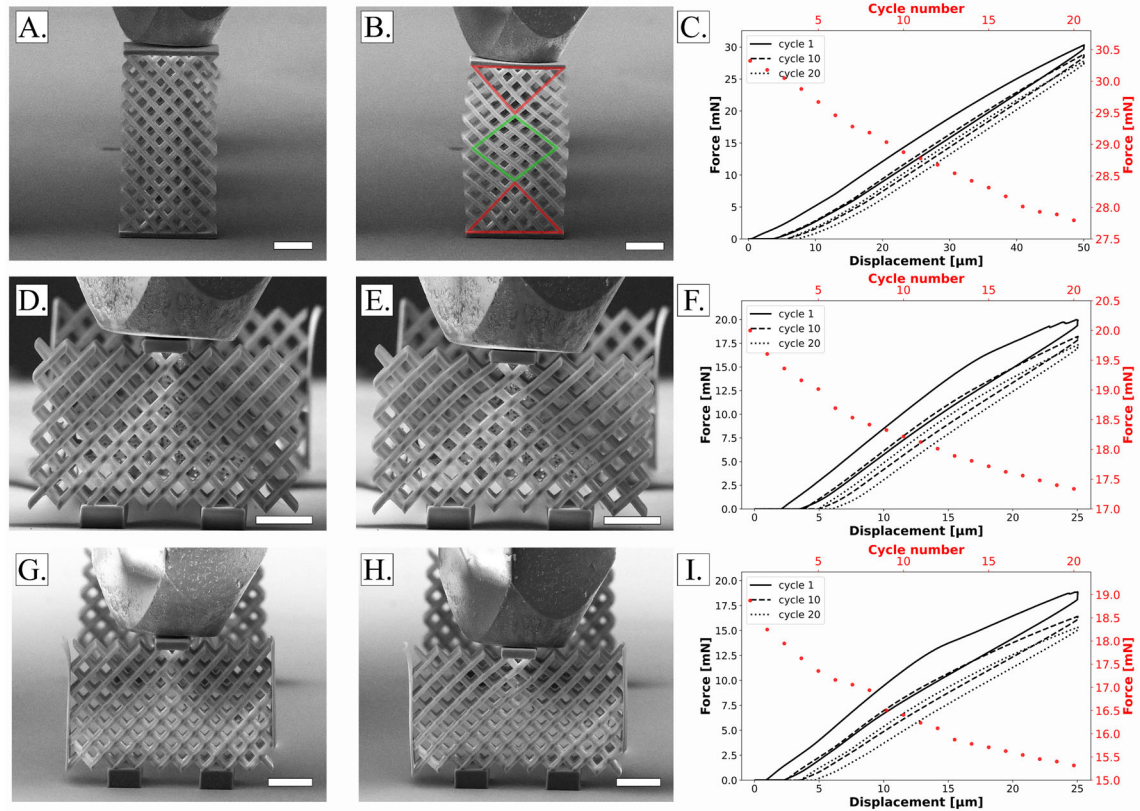


**Fig. 3** 3D micro-metric pantographic metamaterials processed by 2PP and their mechanical properties. SEM images on the left show the unloaded pantographs, while those on the right depict the pantographs under loading using the flat punch. All scale bars indicate a length of 100  $\mu\text{m}$ . For the upright pantographs, the maximum applied displacement was set to 50  $\mu\text{m}$ , and for the horizontally oriented ones, it was set at 25  $\mu\text{m}$ . All loading-unloading tests were conducted with a maximum of 20 cycles. The resulting mechanical behaviors of the 3D micro-metric pantographic metamaterials are illustrated in the graphs on the right. For enhanced visualization, only the force-displacement curves for cycles 1, 10, and 20 are plotted. Dotted plots in red represent the maximum forces applied to achieve the corresponding maximum displacement in each cycle (color figure online)

impact the deformation pattern or the mechanical behavior of horizontally oriented pantographs. Therefore, in this study, the effective stiffness may be primarily determined by the pantographic unit cells.

The mechanical behaviors resulting from the cyclic loading-unloading tests on the 3D micro-metric pantographs are illustrated in Fig. 3, as exemplified by the force-displacement curves measured in the cycles 1, 10, and 20. All specimens clearly exhibit a dissipative response, including residual plastic deformation and nonlinear elastic behavior in the loading phase, along with a relatively broad elastic region.

The broadness of the elastic region is more pronounced in the upright pantograph, as indicated in Fig. 3C. This is likely because all features at the bottom of the structure are fully attached to the plate, which is itself attached to the coverslip, thereby stiffening the overall structure.

To quantify the dissipative response, the dissipated energy  $W_d$  for representative loading-unloading cycle was calculated for each specimen according to the equation  $W_d = W - W_e$ , where  $W$  is the total energy, and  $W_e$  is the elastic energy. Both variables can be calculated as described in Ref. [40]. The calculated values for  $W_d$  are listed in Table 1. Further analysis of the ratio of energy dissipated in representative loading-unloading cycles (see Table 1) hints at a possible limit to the dissipative response further supported by the fact that the total relative plastic deformation across all samples after 20 cycles was consistent, registering approximately 1.6% in relation to the total structure height. Notably, this percentage was determined without accounting for any pre-existing plastic deformation or damage. The maximum force applied also exhibited a consistent relative decrease in all 3D micro-metric pantographs after 20 cycles, ranging from about 3 to 3.5 mN. Notably, the first cycle of the three-point bending tests for both structures already showed plastic deformation, likely induced during the initial loading-unloading test to ensure proper alignment between the flat punch and the

**Table 1** Calculated dissipated energy ( $W_d$ ) in cycles 1, 10 and 20 for studied 3D micro-metric pantographs and the ratio of energy dissipated in representative cycles

Structure	$W_{d,c1}$	$W_{d,c10}$	$W_{d,c20}$	$W_{d,c10} / W_{d,c1}$	$W_{d,c20} / W_{d,c10}$
Upright pantograph	120.20 nJ	71.59 nJ	61.42 nJ	0.60	0.86
Pantograph with sidewalls	55.98 nJ	33.79 nJ	29.43 nJ	0.60	0.87
Pantograph without sidewalls	55.48 nJ	35.11 nJ	28.31 nJ	0.63	0.81

structure. However, confirmation of a limit to the dissipative response would require the development of specific dissipative models.

Of particular interest, the force-displacement diagrams show apparent softening in the most deformed regions of the loading phase. This observation is unexpected in the elastic regime, given that previous studies on pantographic fabrics usually reported on apparent stiffening, and plastic deformations were generally considered as negligible [15]. Furthermore, loading-unloading tests on horizontally oriented pantographic metamaterials showed partial structural failure in the first cycle. According to previous research [15], such failure is marked by at least one abrupt drop in the displacement force, followed by an elastic response, thereby preserving the integrity of the remaining pantographic unit cells. The pantographic metamaterial without sidewalls showed multiple failure features (see Fig. 3F), while the one with sidewalls exhibited a single failure feature (see Fig. 3I).

Various factors could explain the difference in the number of failure features observed. For example, the pantographic structure without sidewalls exhibited greater plastic deformation during the first cycle compared to the one with sidewalls. Another potential factor could be structural imperfections that arise during the fabrication of 3D micro-metric pantographs via 2PP. These structural imperfections could be influenced by variations in the degree of polymerization, which may be due to local impurities in the drop-casted photoresist, or by residual stresses within the structures caused by local shrinkage. Additionally, the degree of polymerization may also differ due to defocusing effects in deeper regions of the photosensitive material, as described in detail in Refs. [41, 42]. In fact, this effect may strongly contribute to structural imperfections since the proposed structures are tall, and the defocusing effect is greater with dry-immersive microscope objectives compared to high numerical aperture microscope objectives that typically require oil as an immersive medium.

However, despite the observed material yielding and damage, the stiffness of the 3D micro-metric pantographs remained nearly constant for both configurations throughout the cyclic loading-unloading tests. This implies that the elastic stiffness is largely independent of the cycle number.

After undergoing in-situ SEM microindentation, the structural failure of 3D micro-metric pantographic metamaterials was analyzed using HIM, as shown in Fig. 4. Neither low-magnification HIM images (see Fig. 4A, D, and G) nor high-magnification images of the upright pantographs showed any visible damage.

However, a detailed examination of individual features in horizontally oriented pantographic unit cells did reveal structural failures. Importantly, all observations made through HIM across all types of 3D micro-metric pantographs were consistent with what was anticipated based on the force-displacement graphs.

Failures in horizontally oriented pantographs primarily occurred in areas where different families of beams intersected through quasi-perfect pivots. For example, pantographic metamaterials without sidewalls exhibited partial detachment of pivots from one set of mutually oriented beams, likely due to torsional forces on the pivots induced by shear forces [17]. These failures were primarily located in the central upper region of the structure but within its volume, near the plate used for applying displacement with a flat punch (see Fig. 4E). As depicted in Fig. 3E and H, these areas experienced greater displacement than those at the bottom or sides of the structure.

Additionally, horizontally oriented pantographs displayed beam constrictions, as shown in Fig. 4F. These constrictions were mainly found in the central upper regions, particularly where mutually orthogonal beams connect through quasi-perfect pivots. They were, however, limited to surface layers and led to the formation of cracks measuring several hundred nanometers. These cracks initiated from beams' edges and extended toward their center.

Interestingly, while constrictions and cracks were observed, no pivot detachment was noted in horizontally orientated pantographic metamaterials with sidewalls (see Fig. 4H and I). The absence of such detachment could be attributed to various factors, including those previously discussed to explain differences in the number of failure features. Another possibility is that these detachments went undetected due to HIM imaging limitations,



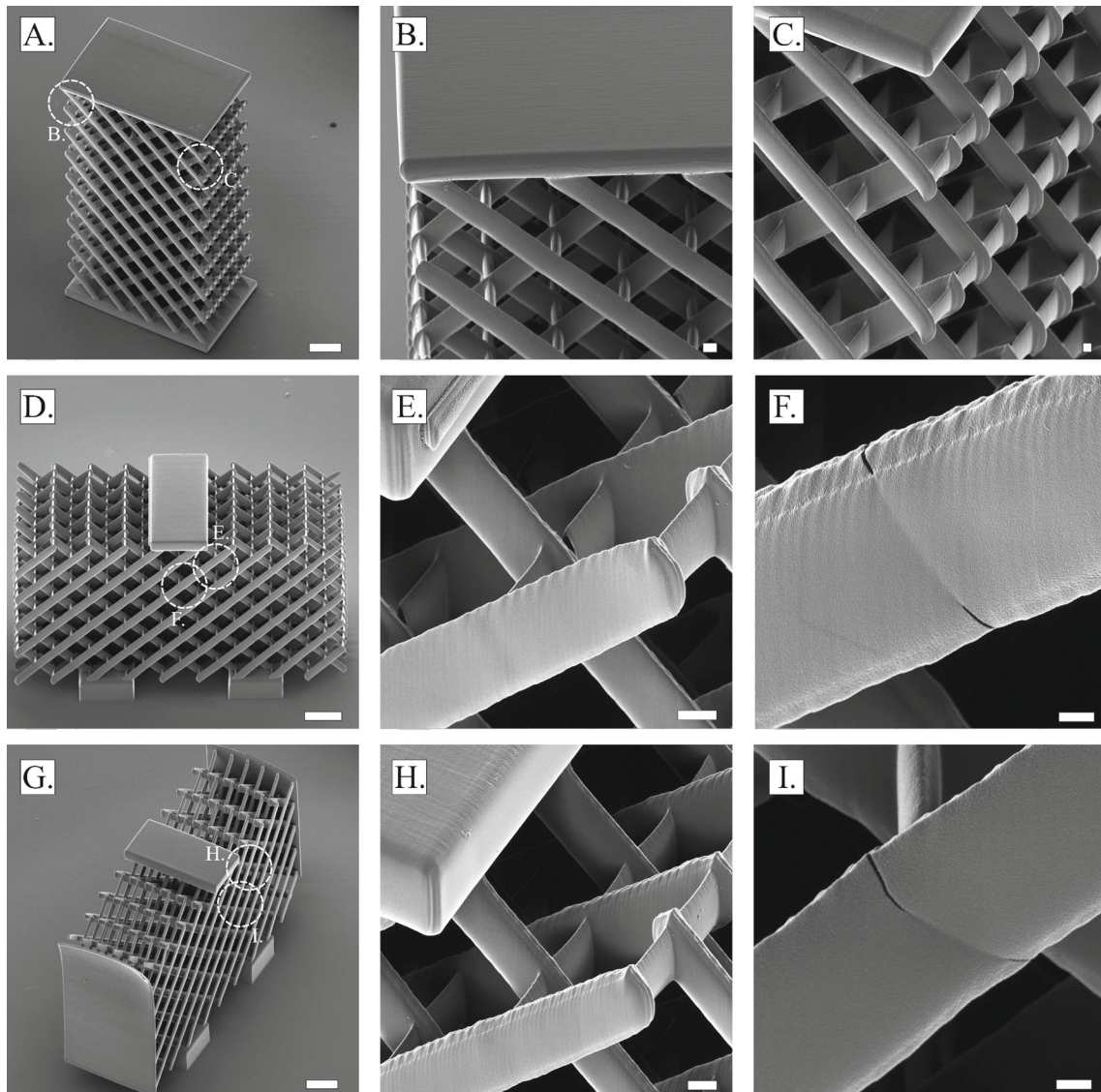


**Fig. 4** Examination of structural failures in 3D micro-metric pantographs following compression tests. HIM images **A–C** illustrate the upright pantograph and its features, while images **D–I** demonstrate the horizontally oriented pantographic metamaterials, both with and without sidewalls, and their features. The scale bars in the images on the left, center, and right correspond to 50  $\mu\text{m}$ , 5  $\mu\text{m}$ , and 2  $\mu\text{m}$ , respectively

particularly since pivot detachment failures occurred within the volume of the horizontally oriented pantographs without sidewalls.

Lastly, it should be noted that although the pivots appear round in the computer model (see Fig. 1), they are actually ellipsoidal in the fabricated specimens. This discrepancy is attributed to the nature of 2PP, where the voxel used for local photoresist processing is elongated along the direction of laser beam focus. Such a geometrical inconsistency could potentially affect the damage mechanisms, as described in Ref. [17].

## 5 Discussion and conclusion

Aiming to advance the field of pantographs as metamaterials, this paper explored the mechanical properties of 3D micro-metric pantographic metamaterials at an extremely small scale. The structures were designed in various configurations by arranging 2D pantographic fabrics in multiple layers. Specifically, the study considered three different types of 3D micro-metric pantographic structures with quasi-perfect pivots: one



upright structure and two horizontally oriented structures, characterized by the presence or absence of lateral reinforcements. The relatively large structures were manufactured with high resolution using 2PP. Afterwards, the mechanical properties of the structures were investigated under cyclic loading conditions using in-situ SEM microindentation. Finally, HIM was used post-testing to assess structural failure.

The primary objective of the study was to determine whether 3D micro-metric pantographs exhibit the same mechanical behavior as scale-independent pantographic fabrics in 2D, thus qualifying them as metamaterials. Additionally, due to the increasing importance of external forces and material properties at the micro-/nanoscale from intermolecular interactions, it was necessary to elucidate differences in load–displacement behavior, specifically through three-point bending tests and compression tests. These tests also aimed to understand the effect of lateral reinforcements on the deformation patterns of pantographic structures.

It can be concluded that the manufactured 3D micro-metric pantographic structures exhibit mechanical behavior that qualitatively resembles that of scale-independent 2D pantographic fabrics [15, 17–22]. This includes their resilience against damage and their distinctive deformation patterns, which can be described using second-gradient type continuum modeling [12–14]. Such observation strengthens the hypothesis that pantographic structures are proper metamaterials.

Notably, loading-unloading tests on horizontally oriented pantographic structures showed, similar to 2D pantographs, partial structural failure in the first cycle evidenced by at least one abrupt drop in the displacement force, followed by an elastic response (see Fig. 3F and I). This behavior preserved the integrity of the remaining pantographic unit cells, indicating that pantographic metamaterials maintain their resilience properties at extremely small length scales, conferred by their topology rather than by the nature, whether ductile or brittle, of their base materials.

In this context, the damage behavior in horizontally oriented 3D pantographs also aligns with findings reported in Ref. [17], where the damage was primarily observed at junctions where different families of beams connect through quasi-perfect pivots (compare Fig. 4). In contrast, the absence of sidewalls does not significantly impact the mechanical behavior. Instead, it was observed that upright pantographs could withstand higher forces, likely because the compression plates block the most significant deformation mode, which is shear.

Of particular interest was that the present work also revealed complex behavior of 3D micro-metric pantographic metamaterials, which may be highly interesting for future studies on 3D pantographs and their potential applications. One such complex mechanical characteristic is that all specimens displayed a moderate dissipative response, as confirmed by the measured residual plastic deformation.

Based on previous experience with pantographic structures [15, 17–22], it can be assumed that most of the recoverable deformation energy was stored either in the bending of the constituting beams or in the torsion of the quasi-perfect pivots. Indeed, this characteristic typically defines the elastic behavior and results in a concomitant compliant response in pantographic structures, but as noted in Ref. [43], repeated loading and unloading cycles may lead to plastic deformation.

Nevertheless, it is important to highlight that the energy dissipated in representative loading-unloading cycles seems to have a potential limit to the dissipative response. This observation is supported by the consistent total relative plastic deformation across all samples after 20 cycles, which was approximately 1.6% in relation to the total structure height. As a result, the measured dissipation may not appear to occur extemporaneously due to accidental changes in testing conditions or manufacturing variations, nor may it seem to result from a systematic error affecting the measurements. This phenomenon, therefore, warrants theoretical investigation in the future.

Besides the presence of a moderate dissipative response, the force-displacement graphs in Fig. 3 also show apparent softening in the most deformed regions during the loading phase. This behavior is particularly interesting as it is unexpected in the elastic regime, given that previous studies on pantographic fabrics typically reported apparent stiffening. The behavior is unlikely to be due to the extremely small size of each feature, as small micro- or nanostructures used to generate a single unit cell usually result in stiffer responses for the overall structure.

Instead, the softening is assumed to be more likely attributable to anelastic phenomena, whether plastic or viscoelastic in nature, which could depend on the material used to manufacture the pantographs or local structural defects, such as variations in the polymerization degree resulting from defocusing effects of laser radiation [41, 42]. A promising way to study and optimize anelastic phenomena and address fabrication errors in the future may be through dynamically altering the laser power during the structuring of a 3D micro-metric pantograph [34] or considering high-temperature treatment as a post-process, known as calcination [44]. The combination of both approaches would be highly interesting as it may enable the manufacturing

of arbitrary 3D inorganic pantographs with high fidelity with respect to geometrical and material properties. Notably, calcination can not only be combined with 2PP [44] but also with other light/laser-based 3D printing techniques [45], allowing the fabrication of 3D inorganic pantographs across different length scales.

For future theoretical studies, it would be valuable to utilize previously derived mathematical models for three-point bending and compression tests [46,47]. Specifically, modeling the mechanical response's dependence on the number of quasi-static loading-unloading cycles, characterized by the same applied displacement, would be of significant interest [48]. In this context, theoretical analyses could incorporate descriptions of plastic phenomena [49] and damage [50], thereby refining second-gradient continuum models that may enable the description of pantographic metamaterials' behavior even at the micro- and nanoscale.

Additionally, these approaches could be enhanced by employing inverse problem techniques. More specifically, inverse problems for generalized elastic continua may enable the description of size-dependent apparent elastic moduli observed in micro- and nano-scale objects [51], such as the pantographic specimen presented in this work. Furthermore, inverse problem techniques could facilitate the identification of localized damage in structural features through the reconstruction of the axial stiffness of individual components, as proposed by Ref. [52]. Damage identification in structural features could also be pursued by utilizing convolutional neural networks [53].

Finally, upon further examination of the experiments, the presented results greatly demonstrated that 3D micro-metric pantographs exhibit excellent resilience, withstanding large cyclic deformations without significant structural failure. Despite material yielding through moderate plastic deformation or partial structural damage, the overall structural functionality was maintained. Interestingly, this resilience may be influenced by the unique elastic stiffness observed across all specimens, independent of the cycle number.

Such mechanical properties, including resistance to out-of-plane motion, make 3D micro-metric pantographs promising for MEMS applications [54]. Moreover, the unique stiffness and resilience of these pantographic metamaterials render them suitable for energy or damping applications, such as shock absorbers and vibration isolators. Additionally, their mechanical properties could be utilized in sensing applications to detect mechanical system failures.

To advance 3D pantographic metamaterials further at the micro- and nanoscale via 2PP, their mechanical characteristics can be tailored for specific applications using evolutionary algorithms [55,56], or artificial intelligence [57]. Future research could also explore more complex pantographic unit cells featuring bi-pantographic motifs [58] or those that exhibit semi-auxetic or monoclastic deformations [59–61]. In this context, recent advancements in process speed [62,63], approaches to enhance precision and fidelity in 2PP [34], materials [25,37,45], and novel laser sources [64,65] are expected to improve the feasibility of fabricating real-world applications or providing cost-effective rapid prototyping using 2PP in the near future.

**Acknowledgements** This project was supported by the Marie Skłodowska-Curie Actions, under grant agreement No. 101059253, as part of the European Union's Horizon Europe research and innovation programme. Additional support came from the European Union's Horizon 2020 research and innovation programme under grant agreement No. 101007417. Furthermore, the research project was co-funded by the Stavros Niarchos Foundation (SNF) and the Hellenic Foundation for Research and Innovation (H.F.R.I.) under the 5th Call of "Science and Society" Action—"Always Strive for Excellence—Theodore Papazoglou" (Project Number: 9578.). The research also benefited from access provided by the Institute of Electronic Structure and Laser (IESL) at the Foundation for Research and Technology-Hellas (FORTH) in Heraklion, Crete, Greece, within the framework of the NFFA-Europe Pilot Transnational Access Activity (Proposal ID 068). The authors thank Prof. Peter Hosemann, Department of Nuclear Engineering, University of California, Berkeley, for providing access to the in-situ SEM microindentation apparatus. Special thanks are also given to Dr. Frances Allen from the Department of Materials Science and Engineering at the University of California, Berkeley, for her invaluable assistance during HIM imaging. Additionally, the authors thank Mrs. Aleka Manousaki for technical support during SEM imaging.

## Declarations

**Author contributions** The study was conceptualized by G.Z., E.B., I.G., F.D., and M.F. The dimensions of the structures were suggested by E.B. and I.G. G.Z. designed the computer models, synthesized the photosensitive materials, and conducted the manufacturing of 3D micro-metric pantographs via two-photon polymerization. Under the supervision of C.G., the fabricated structures were mechanically characterized through in-situ scanning electron microscopy microindentation by G.Z. and S.M., and helium ion microscopy was performed by S.M. Data processing was conducted by E.B., S.M., and G.Z., and all authors discussed the data. G.Z. and E.B. wrote the manuscript, and all authors commented on the paper. The project was supervised by F.D. and G.Z.

**Data availability** No datasets were generated or analysed during the current study.

**Conflict of interest** The authors declare that there is no conflict of interest regarding the publication of this manuscript.

## References

1. Askari, M., Hutchins, D.A., Thomas, P.J., et al.: Additive manufacturing of metamaterials: a review. *Addit. Manuf.* **36**, 101562 (2020)
2. Fan, J., Zhang, S., Wei, L., Zhang, S.-K., Choi, Z., et al.: A review of additive manufacturing of metamaterials and developing trends. *Mater. Today* **50**, 303–328 (2021)
3. Kadic, M., Milton, G.W., van Hecke, M., et al.: 3D metamaterials. *Nat. Rev. Phys.* **1**, 198–210 (2019)
4. Ai, L., Gao, X.L.: Metamaterials with negative Poisson's ratio and non-positive thermal expansion. *Compos. Struct.* **162**, 70–84 (2017)
5. Bückmann, T., Thiel, M., Kadic, M., et al.: An elasto-mechanical unfeelability cloak made of pentamode metamaterials. *Nat. Commun.* **5**, 4130 (2014)
6. Meza, L.R., Das, S., Greer, J.R.: Strong, lightweight, and recoverable three-dimensional ceramic nanolattices. *Science* **345**, 1322–1326 (2014)
7. Evans, K.E., Nkansah, M., Hutchinson, I., et al.: Molecular network design. *Nature* **353**, 124–124 (1991)
8. Milton, G.W., Cherkaev, A.V.: Which elasticity tensors are realizable? *J. Eng. Mater. Technol.* **117**, 483–493 (1995)
9. Seppecher, P., Alibert, J.-J., dell'Isola, F.: Linear elastic trusses leading to continua with exotic mechanical interactions. In: *Journal of Physics: Conference Series*, vol. 319, p. 012018 (2011)
10. Alibert, J.-J., Seppecher, P., dell'Isola, F.: Truss modular beams with deformation energy depending on higher displacement gradients. *Math. Mech. Solids* **8**, 51–73 (2003)
11. Abdoul-Anziz, H., Seppecher, P.: Homogenization of periodic graph-based elastic structures. *J. de l'École polytechnique-Mathématiques* **5**, 259–288 (2018)
12. dell'Isola, F., Andreaus, U., Placidi, L.: At the origins and in the vanguard of peridynamics, non-local and higher-gradient continuum mechanics: an underestimated and still topical contribution of Gabrio Piola. *Math. Mech. Solids* **20**, 887–928 (2015)
13. dell'Isola, F., Giorgio, I., Pawlikowski, M., et al.: Large deformations of planar extensible beams and pantographic lattices: heuristic homogenization, experimental and numerical examples of equilibrium. *Proc. Math. Phys. Eng. Sci. P Roy. Soc A Math. Phys.* **472**:20150790 (2016)
14. Giorgio, I., dell'Isola, F., Steigmann, D.J.: Second-grade elasticity of three-dimensional pantographic lattices: theory and numerical experiments. *Contin. Mech. Thermodyn.* **35**, 1–13 (2023)
15. dell'Isola, F., Seppecher, P., Spagnuolo, M., et al.: Advances in pantographic structures: design, manufacturing, models, experiments and image analyses. *Contin. Mech. Thermodyn.* **31**, 1231–1282 (2019)
16. Barchiesi, E., Spagnuolo, M., Placidi, L.: Mechanical metamaterials: a state of the art. *Math. Mech. Solids* **24**(1), 212–234 (2019)
17. Spagnuolo, M., Barcz, K., Dell'Isola, F., et al.: Qualitative pivot damage analysis in aluminum printed pantographic sheets: numerics and experiments. *Mech. Res. Commun.* **83**, 47–52 (2017)
18. De Angelo, M., Spagnuolo, M., D'annibale, F., et al.: The macroscopic behavior of pantographic sheets depends mainly on their microstructure: experimental evidence and qualitative analysis of damage in metallic specimens. *Contin. Mech. Thermodyn.* **31**, 1181–1203 (2019)
19. Barchiesi, E., Ganzosch, G., Liebold, C., et al.: Out-of-plane buckling of pantographic fabrics in displacement-controlled shear tests: experimental results and model validation. *Contin. Mech. Thermodyn.* **31**, 33–45 (2019)
20. Misra, A., Lekszycki, T., Giorgio, I., et al.: Pantographic metamaterials show atypical poynting effect reversal. *Mech. Res. Commun.* **89**, 6–10 (2018)
21. dell'Isola, F., Turco, E., Misra, A., et al.: Force-displacement relationship in micro-metric pantographs: experiments and numerical simulations. *Comptes Rendus Mécanique* **347**, 397–405 (2019)
22. Vangelatos, Z., Yildizdag, M.E., Giorgio, I., et al.: Investigating the mechanical response of microscale pantographic structures fabricated by multiphoton lithography. *Extreme Mech. Lett.* **43**, 101202 (2021)
23. Turco, E., Rizzi, N.L.: Pantographic structures presenting statistically distributed defects: numerical investigations of the effects on deformation fields. *Mech. Res. Commun.* **77**, 65–69 (2016)
24. Farsari, M., Chichkov, B.N.: Two-photon fabrication. *Nat. Photonics* **3**, 450–452 (2009)
25. Wang, H., Zhang, W., Ladika, D., et al.: Two-photon polymerization lithography for optics and photonics: fundamentals, materials, technologies, and applications. *Adv. Funct. Mater.* **33**, 2214211 (2023)
26. Zyla, G., Farsari, M.: Frontiers of laser-based 3d printing: a perspective on multi-photon lithography. *Laser Photonics Rev.* **18**, 2301312 (2024)
27. Marini, M., Nardini, A., Martínez Vázquez, R., et al.: Microlenses fabricated by two-photon laser polymerization for cell imaging with non-linear excitation microscopy. *Adv. Funct. Mater.* **33**, 2213926 (2023)
28. Bertoncini, A., Laptanok, S.P., Genchi, L., et al.: 3D-printed high-NA catadioptric thin lens for suppression of XPM background in stimulated Raman scattering microscopy. *J. Biophotonics* **14**, e202000219 (2021)
29. Katsantonis, I., Manousidaki, M., Koulouklidis, A.D., et al.: Strong and broadband pure optical activity in 3d printed THz chiral metamaterials. *Adv. Opt. Mater.* **11**, 2300238 (2023)
30. Tsilipakos, O., Xomalis, A., Kenanakis, G., et al.: Split-cube-resonator-based metamaterials for polarization-selective asymmetric perfect absorption. *Sci. Rep.* **10**, 17653 (2020)
31. Zyla, G., Kovalev, A., Grafen, M., et al.: Generation of bioinspired structural colors via two-photon polymerization. *Sci. Rep.* **7**, 17622 (2017)
32. Zyla, G., Kovalev, A., Gurevich, E.L., et al.: Structural colors with angle-insensitive optical properties generated by Morpho-inspired 2PP structures. *Appl. Phys. A* **126**, 740 (2020)
33. Gonzalez-Hernandez, D., Varapnickas, S., Bertoncini, A., et al.: Micro-optics 3D printed via multi-photon laser lithography. *Adv. Opt. Mater.* **11**, 2201701 (2023)
34. Zyla, G., Göran, M., Nolvi, A., et al.: 3d micro-devices for enhancing the lateral resolution in optical microscopy. *Light Adv. Manuf.* **5**, 1–14 (2024)

35. Ovsianikov, A., Viertl, J., Chichkov, B., et al.: Ultra-low shrinkage hybrid photosensitive material for two-photon polymerization microfabrication. *ACS Nano* **2**, 2257–2262 (2008)
36. Rekštytė, S., Jonavičius, T., Gailevičius, D., et al.: Nanoscale precision of 3D polymerization via polarization control. *Adv. Opt. Mater.* **4**, 1209–1214 (2016)
37. Ladika, D., Noirbent, G., Dumur, F., et al.: Synthesis and application of triphenylamine-based aldehydes as photo-initiators for multi-photon lithography. *Appl. Phys. A* **128**, 745 (2022)
38. Bumstead, J.R., Park, J.J., Rosen, I.A., et al.: Designing a large field-of-view two-photon microscope using optical invariant analysis. *Neurophotonics* **5**, 025001 (2018)
39. Pathak, S., Cambaz, Z.G., Kalidindi, S.R., et al.: Viscoelasticity and high buckling stress of dense carbon nanotube brushes. *Carbon* **47**, 1969–1976 (2009)
40. Xingdong, S., Lijia, L., Yue, G., et al.: Influences of organic component on mechanical property of cortical bone with different water content by nanoindentation. *AIP Adv.* **8**, 035003 (2018)
41. Horváth, B., Ormos, P., Kelemen, L.: Nearly aberration-free multiphoton polymerization into thick photoresist layers. *Micro-machines* **8**, 219 (2017)
42. Stichel, T., Hecht, B., Houbertz, R., et al.: Compensation of spherical aberration influences for two-photon polymerization patterning of large 3d scaffolds. *Appl. Phys. A* **121**, 187–191 (2015)
43. Ciallella, A., Giorgio, I., Barchiesi, E., et al.: A 3d pantographic metamaterial behaving as a mechanical shield: experimental and numerical evidence. *Mater. Design* **237**, 112554 (2024)
44. Balčas, G., Malinauskas, M., Farsari, M., et al.: Fabrication of glass-ceramic 3d micro-optics by combining laser lithography and calcination. *Adv. Funct. Mater.* **33**(39), 2215230 (2023)
45. Zhang, W., Li, Z., Dang, R., et al.: Suppressed size effect in nanopillars with hierarchical microstructures enabled by nanoscale additive manufacturing. *Nano Lett.* **23**, 8162–8170 (2023)
46. Yildizdag, M.E., Barchiesi, E., dell’Isola, F.: Three-point bending test of pantographic blocks: numerical and experimental investigation. *Math. Mech. Solids* **25**, 1965–1978 (2020)
47. Tran, C.A., Gołaszewski, M., Barchiesi, E.: Symmetric-in-plane compression of polyamide pantographic fabrics-modelling, experiments and numerical exploration. *Symmetry* **12**, 693 (2020)
48. Kadkhodaei, M., Pawlikowski, M., Drobnicki, R., et al.: Modeling of hyperelasticity in polyamide 12 produced by selective laser sintering. *Contin. Mech. Thermodyn.* **35**, 1–10 (2023)
49. Placidi, L., Barchiesi, E., dell’Isola, F., et al.: On a hemi-variational formulation for a 2D elasto-plastic-damage strain gradient solid with granular microstructure. *Math. Eng.* **5**, 1–24 (2022)
50. Placidi, L., Barchiesi, E., Misra, A.: A strain gradient variational approach to damage: a comparison with damage gradient models and numerical results. *Math. Mech. Complex Syst.* **6**, 77–100 (2018)
51. Fedele, R., Placidi, L., Fabbrocino, F.: A review of inverse problems for generalized elastic media: formulations, experiments, synthesis. *Continuum Mech. Thermodyn.* n.a. (2024)
52. Bilotta, A., Morassi, A., Turco, E.: The use of quasi-isospectral operators for damage detection in rods. *Meccanica* **53**, 319–345 (2018)
53. Bilotta, A., Morassi, A., Turco, E.: Damage identification for steel-concrete composite beams through convolutional neural networks. *J. Vib. Control* **30**, 876–889 (2024)
54. Chang, Y., Wei, J., Lee, C.: Metamaterials—from fundamentals and MEMS tuning mechanisms to applications. *Nanophotonics* **9**, 3049–3070 (2020)
55. Vangelatos, Z., Sheikh, H.M., Marcus, P.S., et al.: Strength through defects: a novel Bayesian approach for the optimization of architected materials. *Sci. Adv.* **7**, eabk2218 (2021)
56. Meier, T., Li, R., Mavrikos, S., et al.: Obtaining auxetic and isotropic metamaterials in counterintuitive design spaces: an automated optimization approach and experimental characterization. *Npj. Comput. Mater.* **10**, 3 (2024)
57. Pengcheng, J., Jochen, M., Raney, J.R., et al.: Mechanical metamaterials and beyond. *Nat. Commun.* **14**, 6004 (2023)
58. Barchiesi, E., dell’Isola, F., Hild, F.: The validation of homogenized modeling for bi-pantographic metamaterials via digital image correlation. *Int. J. Solids Struct.* **208**, 49–62 (2021)
59. Alessandro, C., Gabriele, L.V., Antoine, V., et al.: Deformation mode in 3-point flexure on pantographic block. *Int. J. Solids Struct.* **265–266**, 112129 (2023)
60. Stilz, M., Eugster, S.R., Harsch, J., et al.: A second-gradient elasticity model and isogeometric analysis for the pantographic ortho-block. *Int. J. Solids Struct.* **280**, 112358 (2023)
61. Stilz, M., Plappert, D., Gutmann, F., et al.: A 3d extension of pantographic geometries to obtain metamaterial with semi-auxetic properties. *Math. Mech. Solids* **27**(4), 673–686 (2022)
62. Saha, S.K., Wang, D., Nguyen, V.H., et al.: Scalable submicrometer additive manufacturing. *Science* **366**, 105–109 (2019)
63. Somers, P., Liang, Z., Johnson, J.E., et al.: Rapid, continuous projection multi-photon 3D printing enabled by spatiotemporal focusing of femtosecond pulses. *Light Sci. Appl.* **10**, 199 (2021)
64. Zyla, G., Surkamp, N., Gurevich, E.L., et al.: Two-photon polymerization with diode lasers emitting ultrashort pulses with high repetition rate. *Opt. Lett.* **45**, 4827–4830 (2020)
65. Skliutas, E., Samsonas, D., Čiburys, A., et al.: X-photon laser direct write 3d nanolithography. *Vir. Phys. Prototyp.* **14**, e2228324 (2023)

**Publisher’s Note** Springer Nature remains neutral with regard to jurisdictional claims in published maps and institutional affiliations.

Springer Nature or its licensor (e.g. a society or other partner) holds exclusive rights to this article under a publishing agreement with the author(s) or other rightsholder(s); author self-archiving of the accepted manuscript version of this article is solely governed by the terms of such publishing agreement and applicable law.